ADVANCES IN ATMOSPHERIC SCIENCES, VOL. 32, JUNE 2015, 794–806

Asian Summer Monsoon Onset in Simulations and CMIP5 Projections Using Four Chinese Climate Models

ZOU Liwei* and ZHOU Tianjun

State Key Laboratory of Numerical Modeling for Atmospheric Sciences and Geophysical Fluid Dynamics, Institute of Atmospheric Physics, Chinese Academy of Sciences, Beijing 100029

(Received 17 March 2014; revised 10 October 2014; accepted 24 October 2014)

ABSTRACT

The reproducibility and future changes of the onset of the Asian summer monsoon were analyzed based on the simulations and projections under the Representative Concentration Pathways (RCP) scenario in which anthropogenic emissions continue to rise throughout the 21st century (i.e. RCP8.5) by all realizations from four Chinese models that participated in the Coupled Model Intercomparison Project Phase 5 (CMIP5). Delayed onset of the monsoon over the Arabian Sea was evident in all simulations for present-day climate, which was associated with a too weak simulation of the low-level Somali jet in May. A consistent advanced onset of the monsoon was found only over the Arabian Sea in the projections, where the advanced onset of the monsoon was accompanied by an increase of rainfall and an anomalous anticyclone over the northern Indian Ocean. In all the models except FGOALS-g2, the enhanced low-level Somali jet transported more water vapor to the Arabian Sea, whereas in FGOALS-g2 the enhanced rainfall was determined more by the increased wind convergence. Furthermore, and again in all models except FGOALS-g2, the equatorial SST warming, with maximum increase over the eastern Pacific, enhanced convection in the central West Pacific and reduced convection over the eastern Indian Ocean and Maritime Continent region, which drove the anomalous anticyclonic circulation over the western Indian Ocean. In contrast, in FGOALS-g2, there was minimal (near-zero) warming of projected SST in the central equatorial Pacific, with decreased convection in the central West Pacific and enhanced convection over the Maritime Continent. The broader-scale differences among the models across the Pacific were related to both the differences in the projected SST pattern and in the present-day simulations.

Key words: Asian summer monsoon, onset, climate projection, Chinese climate models

Citation: Zou, L. W., and T. J. Zhou, 2015: Asian summer monsoon onset in simulations and CMIP5 projections using four Chinese climate models. *Adv. Atmos. Sci.*, **32**(6), 794–806, doi: 10.1007/s00376-014-4053-z.

1. Introduction

The Asian monsoon system is one of the most powerful in the world. Its evolution and variability affect not only the local agriculture, ecosystems, economics and society, but also the climate on a global scale (e.g. Ding and Wang, 2005). The Asian monsoon is characterized by a strong annual cycle with a rainy summer and dry winter. Understanding and forecasting changes of the monsoon's onset is of great importance, since a late or early onset of the monsoon may have significant impacts on agriculture (Webster et al., 1998).

Recent studies on the monsoon's changes have shown that the Asian summer monsoon exhibits a salient advance by 2–4 pentads after 1993/94, extending from the Bay of the Bengal to the South China Sea (Kajikawa et al., 2012). Advances in monsoon onset over the Arabian Sea and Bay of the Bengal have also been revealed (Wang et al., 2012; Yu et al., 2012). The causes of such advances in Asian monsoon onset are still under debate. Kajikawa et al. (2012) and Wang et al. (2012) ascribed it to enhanced heat contrast between the Asian continent and the tropical Indian Ocean, while Kajikawa and Wang (2012) suggested that SST warming over the western Pacific is the key factor that favors advanced monsoon onset over the South China Sea. A recent study argues that the advances in Asian summer monsoon onset during the last three decades are closely tied to the decadal mean state change in the Pacific, characterized by a distinct La Niña-like pattern (Xiang and Wang, 2013).

Climate system models have been widely employed to reproduce the annual cycle of the Asian monsoon. For example, the climatological intraseasonal oscillation of precipitation over the Asian–western Pacific region was reasonably reproduced in a multi-model ensemble (MME) of 10 atmospheric general circulation models (AGCMs) (Kang et al., 2002). Sperber et al. (2013) compared the performance of 25 Coupled Model Intercomparison Project Phase 5 (CMIP5) models and 22 CMIP Phase 3 (CMIP3) models in simulating the Asian summer monsoon at various time scales. Overall, the CMIP5 MME mean showed better performance in simu-

* Corresponding author: ZOU Liwei
Email: zoulw@mail.iap.ac.cn

lating the onset of the monsoon than the CMIP3 MME mean in terms of the pattern correlation, but the onset of the monsoon over India was typically too late in both MMEs.

Information regarding future changes of monsoon onset under global warming scenarios is helpful for decision-making and impact studies. Although the observed onset of the Asian summer monsoon has exhibited an advance in recent decades, projected future changes do not show the same features. For example, based on projections under the Special Report on Emissions Scenarios (SRES) A1B scenario derived from 19 CMIP3 models, Inoue and Ueda (2011) found that the onset of monsoon over the Bay of the Bengal, the Indochina Peninsula and the South China Sea could be delayed by 5 to 10 days by the end of the 21st century, associated with a delay in the reversal of upper-tropospheric meridional thermal contrast. Zhang et al. (2012) found that monsoon onset tends to delay over the tropical Indian Ocean, Maritime Continent and Indochina Peninsula in the majority of models under warming scenarios. Importantly, the projection of changes in monsoon onset is sensitive to the way in which the monsoon onset is defined. Kitoh et al. (2013) analyzed the future projections under RCP scenarios of 29 CMIP5 models, and the results suggested that monsoon retreat will be delayed but monsoon onset will either advance or show no change at the end of 21st century.

Recognizing the importance of climate models in climate predictions and projections, the Chinese climate research community has been involved in the development of climate models since the late 1970s. Zhou et al. (2014a) reviewed the development of coupled earth/climate system models in China during approximately the past 20 years from the CMIP perspective. There was only one Chinese climate model that participated in CMIP1; however, in the latest phase of the project (CMIP5) there are five models developed in China, and there will be even more climate models from China participating in CMIP6 in the near future (Zhou et al., 2014a). To comprehensively evaluate the performance of current Chinese earth/climate system models, several climate modeling centers in China have jointly initiated a collaborative research project to further encourage collaboration in future model developments. The general performances of Chinese models have been systematically assessed using some observational metrics in Zhou et al. (2014b). The models broadly show reasonable performance in simulating the SST mean state, seasonal cycle, the spatial pattern of Madden–Julian oscillation amplitude and tropical Genesis Potential Index, the global monsoon precipitation pattern, and the SST anomalies related to the El Niño–Southern Oscillation (ENSO) and Pacific Decadal Oscillation (Zhou et al., 2014b). However, the simulations and projections of Asian summer monsoon onset in these Chinese models have yet to be evaluated and compared. We address this knowledge gap in the current paper, and also include an example of moisture budget analysis to examine the monsoon onset changes over a specific region.

The remainder of the paper is organized as follows. Section 2 describes the data and methods. The results, including historical simulations of monsoon onset and future projections, are presented in section 3. Section 4 summarizes the major findings of the study and provides some further discussion.

2. Data and methods

2.1. *Model data and observational data*

Historical simulations from 1981–2005 derived from four Chinese models that participated in CMIP5 are used. These four models are BCC-CSM1-1 from the Beijing Climate Center, China Meteorology Administration (Wu et al., 2010, 2014), BNU-ESM from Beijing Normal University (Wu et al., 2013), and two versions of the FGOALS2 model, viz. FGOALS-g2 (Li et al., 2013) and FGOALS-s2 (Bao et al., 2013), from the Institute of Atmospheric Physics (IAP), Chinese Academy of Sciences. These four models have comparable spatial resolutions in their atmospheric components, with FGOALS2 having a slightly higher resolution. FGOALS-g2 and FGOALS-s2 share the same oceanic component, while BCC-CSM and BNU-ESM employ different versions of the same oceanic model. More detailed model information can be found in Table 1.

The future projections by these four models under the Representative Concentration Pathways (RCP) scenario in which anthropogenic emissions continue to rise throughout the 21st century, resulting in a radiative forcing of 8.5 W m^{-2} (i.e. RCP8.5), are employed to investigate the possible future changes in the Asian summer monsoon. We focus on the last 25 years of the 21st century (2075–2099) and use all the available realizations of these models. For FGOALS-s2, three realizations are employed, while for the other three models one realization is available. The three realizations of FGOALS-s2 are referred to as "FGOALS-s2 r1", "FGOALS-s2 r2", and "FGOALS-s2 r3", respectively.

The following datasets are used to evaluate the models' performances in terms of the present-day climate: (1) pentad precipitation data from the Global Precipitation Climatology Project (GPCP; Adler et al., 2003); (2) pentad precipitation derived from the Climate Prediction Center (CPC) Merged Analysis of Precipitation (CMAP) (Xie and Arkin, 1997); (3) observational SST derived from the Hadley Centre Global Sea Ice and Sea Surface Temperature (HadISST) dataset (Rayner et al., 2003); (4) monthly mean circulation fields [e.g., zonal wind (u), meridional wind (v), specific humidity (q)] derived from the Interim European Centre for Medium-Range Weather Forecasts (ECMWF) Re-Analysis (ERAIM) (Dee et al., 2011). For simplicity, the rainfall dataset and the reanalysis-derived circulation dataset are referred to as "observation" in the following discussion.

2.2. *Methods*

Monsoon onset is defined following the method of Wang and Lin (2002). The pentad time series of precipitation are firstly smoothed with a five-pentad running mean, and then the January mean rainfall is subtracted from each pentad to obtain a relative rainfall rate series. Monsoon onset is defined

Table 1. Institution, model designation, and horizontal and vertical resolutions of the four Chinese climate system models.

Model	Institution	AGCM	OGCM	Land	Sea ice	Coupler	Reference
BCC-CSM1-1	Beijing Climate Center, China Meteorological Administration	BCC_AGCM2.1 T42L26	MOM4 1°(lon)×1.33° (lat) L40	BCC_AVIM 128 × 60 L10+5	SIS 1°(lon)×1.33° (lat)	CPL6	Wu et al. (2014)
BNU-ESM	College of Global Change and Earth System Science, Beijing Normal University	CAM3.5 T42L26	MOM4p1 360 × 200 L50	CoLM+BNUDGVM T42 L10+5	CICE4.1 360 × 200	CPL6.5	Wu et al. (2013)
FGOALS-g2	LASG, Institute of Atmospheric Physics and CESS, Tsinghua University	GAMIL 2.0 128× 60 L26	LICOM 2.0 360 × 196 L30	CLM3 128 × 60 L10+5	CICE_LASG 360 × 200 L4	CPL6	Li et al. (2013)
FGOALS-s2	LASG, Institute of Atmospheric Physics	SAMIL 2.0 128× 108 L26	LICOM 2.0 360 × 196 L30	CLM3 128 × 60 L10+5	CICE_LASG 360 × 196 L4	CPL6	Bao et al.(2013)

as the first pentad in which the relative rainfall rate exceeds 5 mm d^{-1} during May–September. This definition has been widely used in studies on monsoon annual cycles (e.g. Xiang and Wang, 2013; Sperber et al., 2013; Kitoh et al., 2013).

3. Results

3.1. *Evaluation of simulated Asian monsoon onset for present-day climate*

Figure 1 shows the spatial distributions of pentads of Asian monsoon onset derived from simulations and observation. In the observation, the monsoon is first established over Southeast Asia (Matsumoto, 1997), and then over the South China Sea and to the southwest of the Indian subcontinent. Later, the South China Sea monsoon gradually progresses northward to North China. The final established monsoon is the western North Pacific summer monsoon. These characteristics are discussed at length in Wang and Lin (2002). The features are consistent between GPCP and CMAP, with a spatial pattern correlation coefficient (SCC) of 0.76. However, compared with GPCP, the extension of the western North Pacific monsoon in CMAP is farther eastward and the associated onset occurs earlier.

In all six experiments, the simulated monsoon onset firstly (finally) occurs over Southeast Asia (western North Pacific). These features are consistent with the observations. FGOALS-g2 has the highest model skill among these experiments in terms of SCC (Fig. 1). However, FGOALS-g2 lacks any onset over much of India, Southeast Asia, and the South China Sea. The simulated monsoon onsets by BNU-ESM, FGOALS-g2 and FGOALS-s2 are later than in the observation over the western North Pacific and Southeast Asia, while they are earlier in BCC-CSM. Some common biases are also evident in the four modes, i.e. the underestimated (overestimated) extension of monsoon over eastern China, Korea, and Japan (western Pacific Ocean). These biases are also found in most other CMIP5 models (Sperber et al., 2013).

It is found that the monsoon onset over the Arabian Sea (5°–15°N, 65°–75°E) occurs later than that observed in all six experiments. The regional averaged onset over the Arabian Sea is pentad 29.6 (28.9) in GPCP (CMAP), while it is later than pentad 31 in all six experiments (33.6 in BCC-CSM, 36.2 in BNU-ESM, 31.6 in FGOALS-g2, 31.4 in FGOALS-s2 r1, 31.9 in FGOALS-s2 r2, and 31.3 in FGOALS-s2 r3). Since the observed monsoon onset mainly occurs in late-May, examining the simulated mean circulation field in May is helpful for understanding why all the models tend to simulate a delayed monsoon onset. Figure 2 shows the spatial distributions of 850-hPa low-level wind and rainfall in May derived from observation and the corresponding biases derived from the simulations. In the observation, the low-level Somali cross-equatorial flows (CEFs) reach north of 10°N (Fig. 2a), while the simulated Somali CEFs mainly locate south of 5°N and the associated intensities are too weak compared with the observation (figures not shown). Among the six experiments, BNU-ESM has the weakest Somali CEF, and the

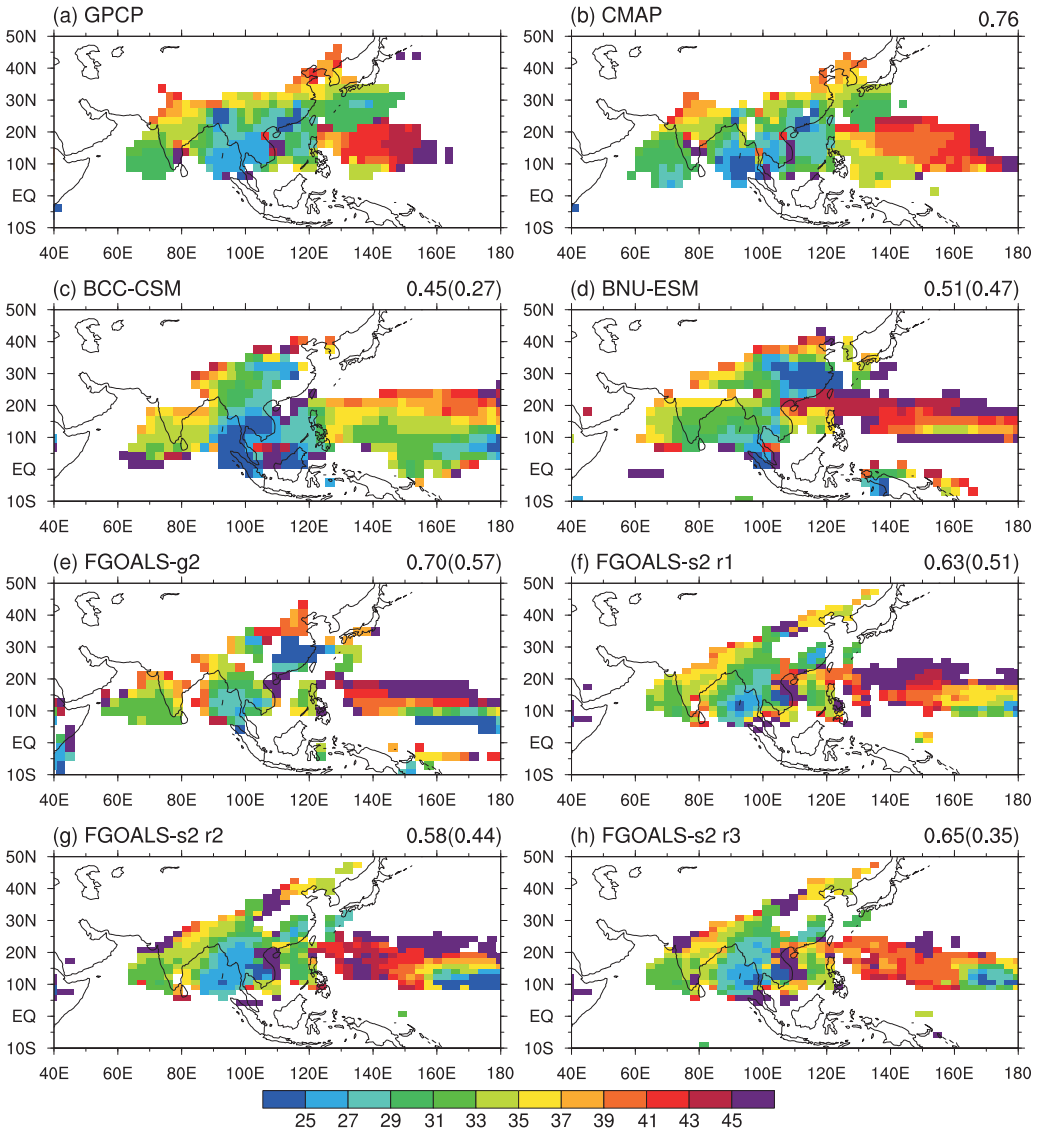

Fig. 1. Spatial distributions of the Asian summer monsoon onset pentad derived from (a) GPCP, (b) CMAP, (c) BCC-CSM, (d) BNU-ESM, (e) FGOALS-g2, (f) FGOALS-s2 r1, (g) FGOALS-s2 r2, and (h) FGOALS-s2 r3. "r1", "r2", and "r3" denote the three realizations of FGOALS-s2, respectively. The data of coupled models are derived from the 20th century historical climate simulations during 1981–2005. The results are presented with the grid of individual model/observation. Note that pentad 30 is the end of May. The numbers shown in the upper-right corner of each plot are the spatial pattern correlation coefficients with GPCP data and with CMAP data, the latter being the number in brackets.

evident northeasterly biases are found over the northern Indian Ocean (Fig. 2c). Since the Somali CEF plays a dominant role in moisture transport, the weakly simulated Somali CEFs lead to dry biases over the Arabian Sea in all six experiments (Figs. 2b–g), leading to a delayed monsoon onset over the Arabian Sea.

The weak Somali CEFs in the simulations are associated with Arabian Sea cold SST biases. Figure 3 shows the spatial distributions of simulated SST biases in boreal spring with respect to HadISST. The cold SST biases over the Arabian Sea are evident in all six experiments. Levine et al. (2013) examined the extent and impact of cold SST biases in the northern Arabian Sea in the CMIP5 MME. The results showed that such cold SST biases are common in CMIP5 models, and a clear relationship exists between Arabian Sea cold SST biases in boreal spring and weak monsoon rainfall. The Arabian Sea cold SST biases reduce the moisture fluxes over the Arabian Sea (Levine et al., 2013), which will lead to decreases of rainfall and favor delayed monsoon onsets.

3.2. *Projected changes of monsoon onset under RCP 8.5*

Figure 4 shows the projected changes of Asian monsoon onset for the period 2075–2099 under the RCP8.5 scenario relative to 1981–2005. There are some changes in the mon-

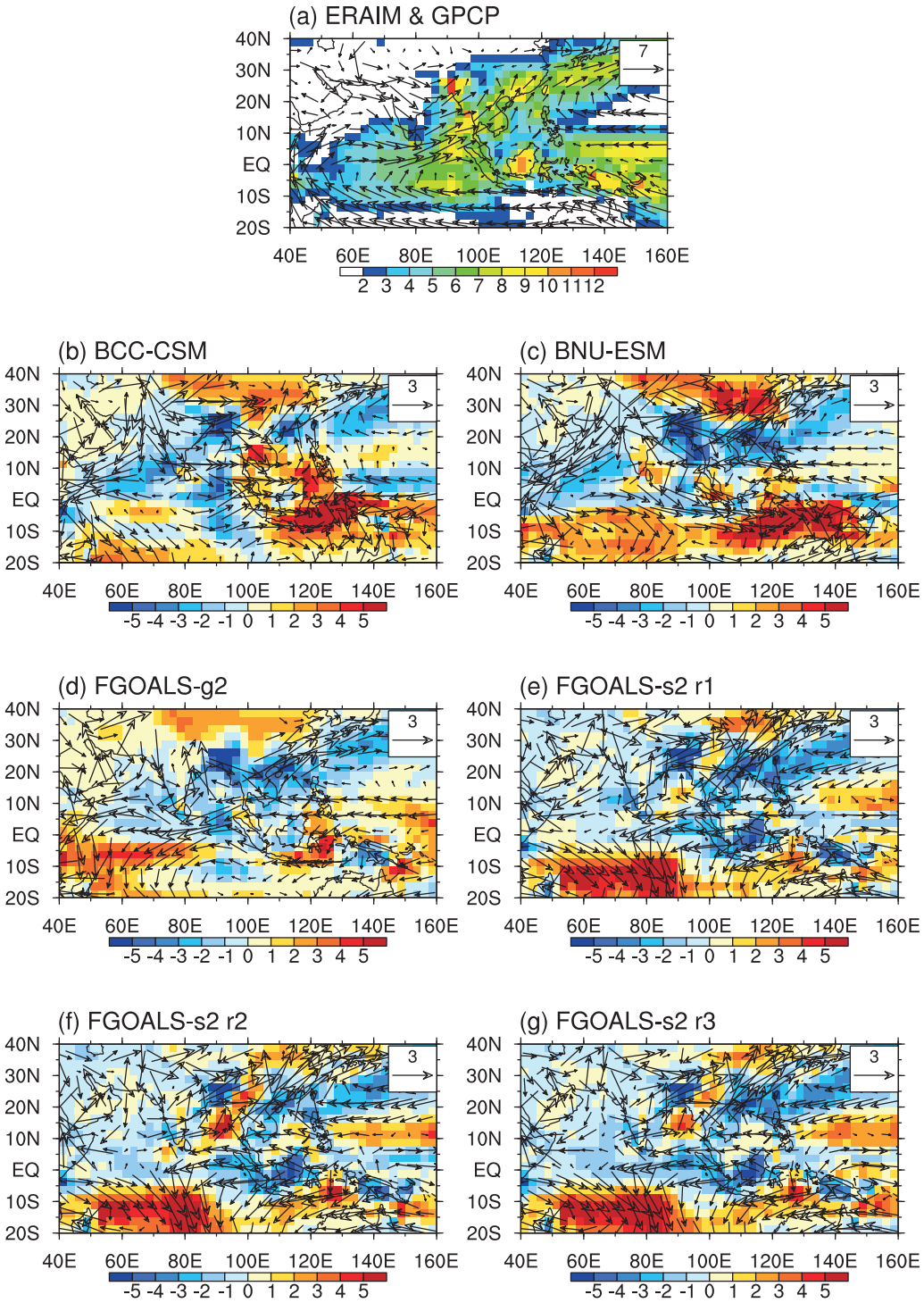

Fig. 2. (a) Spatial distributions of rainfall (shading, mm d^{-1}) and 850-hPa low-level wind in May averaged during 1981–2005 derived from GPCP and ERA-interim, and the corresponding simulated biases (simulations minus the observations) derived from (b) BCC-CSM, (c) BNU-ESM, (d) FGOALS-g2, (e) FGOALS-s2 r1, (f) FGOALS-s2 r2, and (g) FGOALS-s2 r3.

soon domain based on the definition of monsoon onset. At first sight, consistency among all six experiments with regard to the projected changes of monsoon onset is low. For instance, all realizations of FGOALS-s2 project an advanced monsoon onset over the western North Pacific, while the other three models overall exhibit a delayed monsoon onset. For the Indian subcontinent, advanced monsoon onset is found in BCC-CSM, FGOALS-g2, and FGOALS-s2 r1, while a delayed monsoon onset is prominent in BNU-ESM, FGOALS-s2 r2 and r3. For the region of Vietnam/Cambodia,

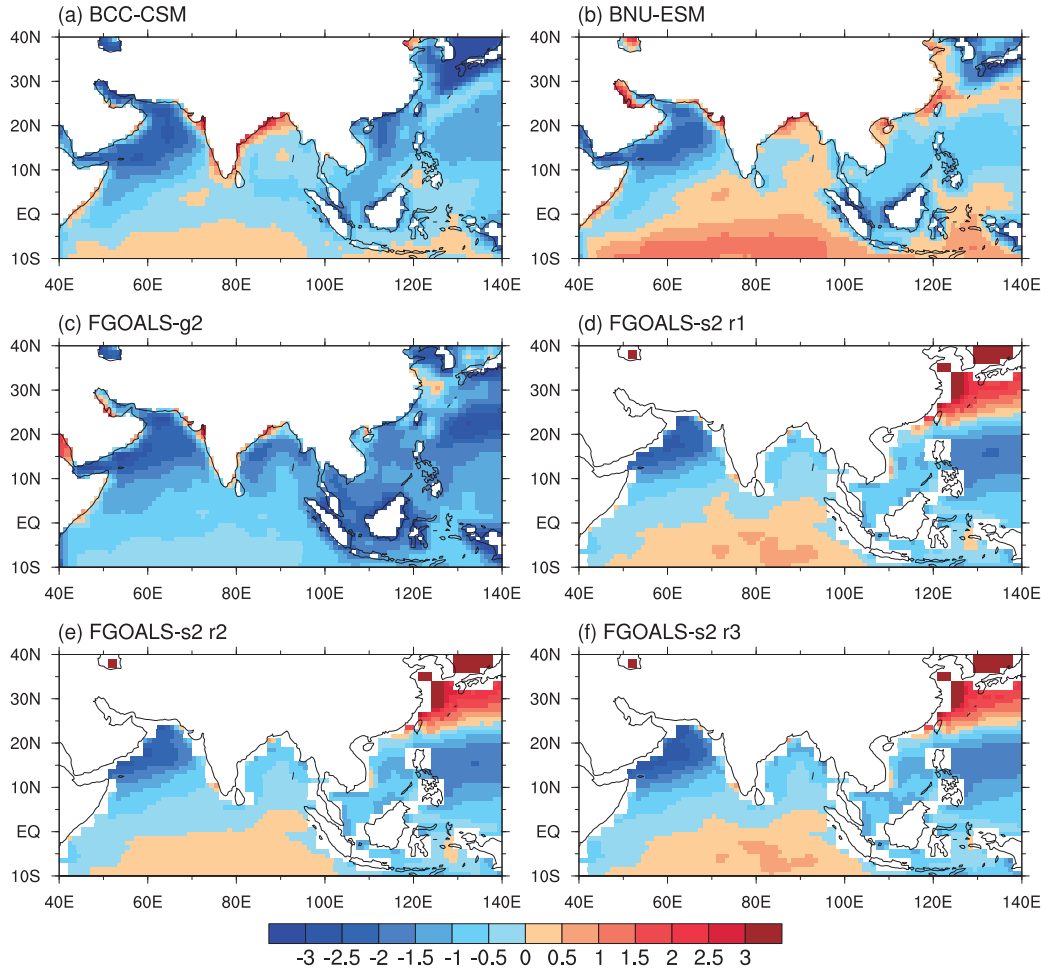

Fig. 3. Spatial distributions of simulated SST biases (°C) in boreal spring with respect to HadISST derived from (a) BCC-CSM, (b) BNU-ESM, (c) FGOALS-g2, (d) FGOALS-s2 r1, (e) FGOALS-s2 r2, and (f) FGOALS-s2 r3.

delayed onset is found in FGOALS-g2 and the three realizations of FGOALS-s2, while such a signal is not evident in BCC-CSM and BNU-ESM.

Based on the results shown in Fig. 4, Fig. 5 further depicts the regional averaged changes in monsoon onset over the Arabian Sea (5°–15°N, 65°–75°E), Bay of Bengal (10°–20°N, 85°–95°E), Southeast Asia (8°–20°N, 100°–110°E), and the western North Pacific (10°–20°N, 125°–160°E) in the results of the six experiments. The monsoon over the Arabian Sea tends to be established one to two pentads earlier than at present, which is a consistent signal among the six experiments. For the monsoon over the Bay of Bengal, delayed onset is found in BNU-ESM and FGOALS-s2 r2, while advanced onset is found in the other experiments, with the largest advance found in FGOALS-g2. For Southeast Asia, the monsoon onset is projected by FGOALS-g2 and FGOALS-s2 to become delayed. Delayed monsoon onset over the Indochina Peninsula has also been found in previous studies based on CMIP3 projections (Inoue and Ueda, 2011; Zhang et al., 2012). In addition, the western North Pacific monsoon tends to be established earlier in FGOALS-s2, while it tends to be later in FGOALS-g2. In the following discussion, we examine why the models tend to project an advanced monsoon onset over the Arabian Sea.

3.3. *Moisture diagnosis of rainfall changes over the Arabian Sea*

Since the monsoon onset over the Arabian Sea occurs in early-June (early-July) in BCC-CSM, FGOALS-g2, FGOALS-s2 (BNU-ESM) for present-day climate, we focus on the projected changes of mean fields in May (June) in BCC-CSM, FGOALS-g2, FGOALS-s2 (BNU-ESM) to examine the changes of large-scale circulations that favor an advanced monsoon onset under the RCP8.5 scenario. Figure 6 shows the projected changes of the 850-hPa wind field and precipitation in May (June) from BCC-CSM, FGOALS-g2, FGOALS-s2 (BNU-ESM) at the end of 21st century. The results are also presented for the three realizations of FGOALS-s2. A pair of anomalous anticyclones is found over the Indian Ocean, with much greater strength over the northern Indian Ocean. The westerly anomalies associated with the northern branch of the anomalous anticyclone over the northern Indian

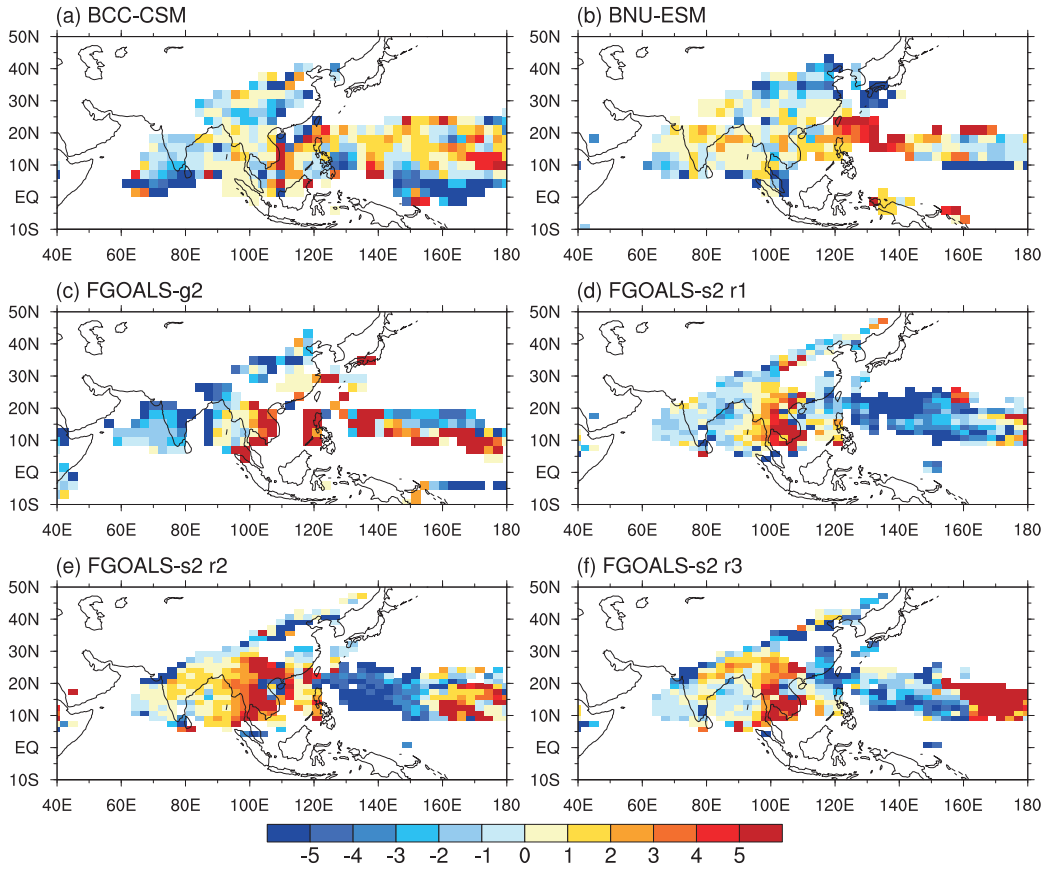

Fig. 4. Spatial patterns of projected Asian summer monsoon onset changes under the RCP8.5 scenario for the period 2075–2099 relative to 1981–2005 (onset pentad for 2075–2099 minus onset pentad for 1981–2005) derived from (a) BCC-CSM, (b) BNU-ESM, (c) FGOALS-g2, (d) FGOALS-s2 r1, (e) FGOALS-s2 r2, and (f) FGOALS-s2 r3. Negative values indicate earlier onset.

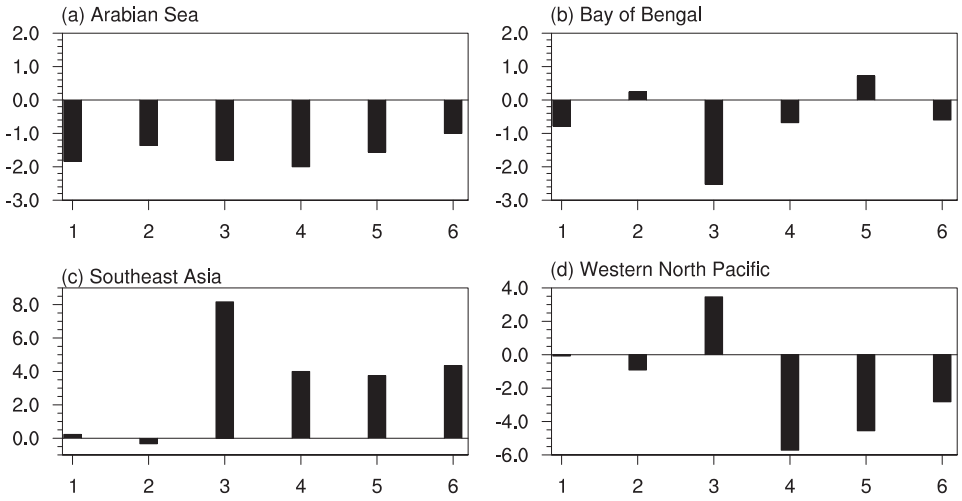

Fig. 5. Regional averaged changes in monsoon onset over the (a) Arabian Sea (5°–15°N, 65°–75°E), (b) Bay of Bengal (10°–20°N, 85°–95°E), (c) Southeast Asia (8°–20°N, 100°–110°E), and (d) western North Pacific (10°–20°N, 125°–160°E) under the RCP 8.5 scenario derived from different experiments. The numbers on the *x*-axis correspond to different models or different realizations: (1) BCC-CSM; (2) BNU-ESM; (3) FGOALS-g2; (4) FGOALS-s2 r1; (5) FGOALS-s2 r2; (6) FGOALS-s2 r3. The time axis is pentads. Negative values indicate earlier onset.

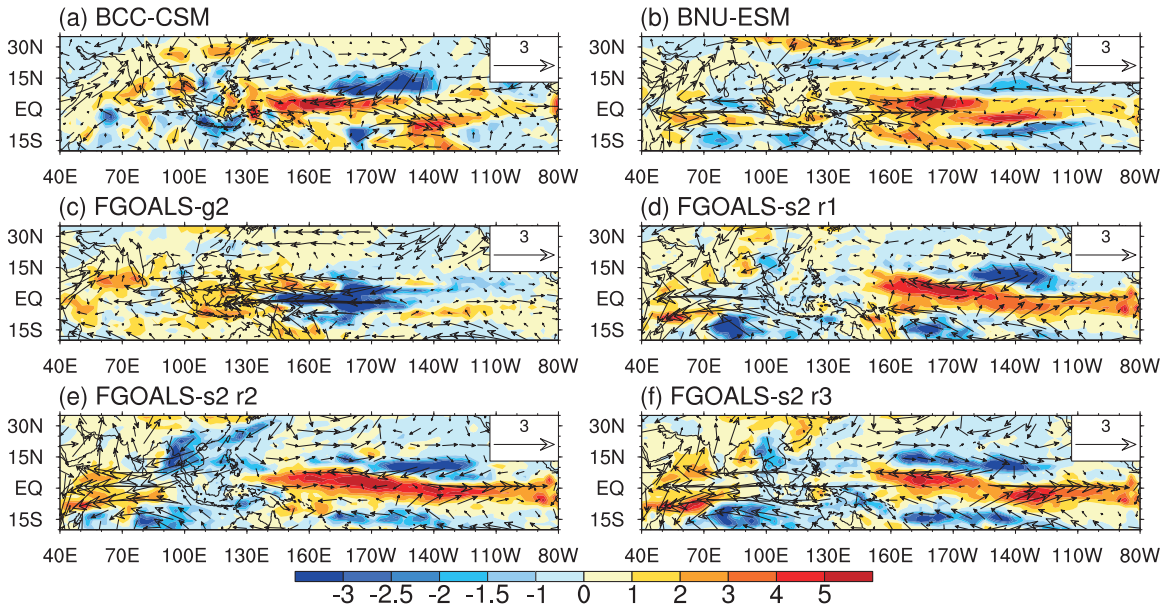

Fig. 6. Projected changes of rainfall (mm d^{-1}) and 850-hPa low-level wind (m s^{-1}) in May (June) for the period 2075–2099 under the RCP 8.5 scenario relative to 1981–2005 derived from (a) BCC-CSM, (b) BNU-ESM, (c) FGOALS-g2, (d) FGOALS-s2 r1, (e) FGOALS-s2 r2, and (f) FGOALS-s2 r3.

Ocean are accompanied by increased precipitation over the Arabian Sea, which favors advanced monsoon onsets since the definition of monsoon onset is solely based on precipitation. Note that the anomalous anticyclone is much weaker in FGOALS-g2 than in the other models.

To reveal the physical linkages between the rainfall changes and the circulation changes over the Arabian Sea (5°–15°N, 65°–75°E), we examine the vertically integrated moisture budget equation shown below:

$$\Delta P = -\Delta\langle \boldsymbol{V}\cdot\nabla q\rangle - \Delta\langle q\nabla\cdot\boldsymbol{V}\rangle + \Delta E\ , \qquad (1)$$

where P is precipitation, $\boldsymbol{V}$ is the horizontal wind vector, q is the specific humidity, E is evaporation, Δ represents the difference between the future and present-day climate simulations (RCP8.5 minus present-day), $\langle\ \rangle$ indicates vertical integration from 1000 to 100 hPa, and ∇ is the horizontal gradient operator. According to Eq. (1), the rainfall changes may be attributed to changes in horizontal moisture advection, moisture convergence associated with mass convergence and surface evaporation.

The diagnosis result (Fig. 7a) shows that the increase of horizontal moisture advection contributes the most to the increase of rainfall over the Arabian Sea, except in FGOALS-g2. In FGOALS-g2, the most important factor is the increase of moisture convergence, while this factor is the second most important factor in the other experiments. The smaller contribution from the moisture advection change in FGOALS-g2 is related to the weaker circulation changes shown in Fig. 6c. The large easterlies biases in FGOALS-g2 over the Arabian Sea in present-day climate (Fig. 2d) may also favor weaker moisture advection changes. The surface evaporation change also contributes positively to the rainfall increase but the amplitude is much smaller than for the other two terms.

As both the changes in atmospheric moisture and circulation affect the moisture advection and moisture convergence, we further decompose these two terms into three components to reveal the relative contributions. The changes of horizontal moisture advection and moisture convergence can be decomposed into three terms, as shown below:

$$-\Delta\langle \boldsymbol{V}\cdot\nabla q\rangle = -\langle \boldsymbol{V}_{\rm pd}\cdot\Delta(\nabla q)\rangle - \langle(\nabla q)_{\rm pd}\cdot\Delta\boldsymbol{V}\rangle - \langle\Delta(\nabla q)\cdot\Delta\boldsymbol{V}\rangle \qquad (2)$$

$$-\Delta\langle q\nabla\cdot\boldsymbol{V}\rangle = -\langle\Delta q(\nabla\cdot\boldsymbol{V}_{\rm pd})\rangle - \langle q_{\rm pd}\Delta(\nabla\cdot\boldsymbol{V})\rangle - \langle\Delta q\Delta(\nabla\cdot\boldsymbol{V})\rangle\ . \qquad (3)$$

The first term on the right-hand side of Eqs. (2) and (3) is associated with the change of water vapor, while the second term is associated with circulation change. The third term is a nonlinear term including the contribution of both moisture and circulation changes. The subscript "pd" denotes the present-day climate. The diagnosis results (Figs. 7b and c) indicate that the increase of moisture advection due to the change of circulation plays a crucial role in enhancing rainfall over the Arabian Sea. In FGOALS-g2, the increase of moisture convergence due to the increase of wind convergence plays an important role.

In summary, the above moisture budget analyses demonstrate that the anomalous circulation changes over northern Indian Ocean in these four models enhance either the wind convergence (in FGOALS-g2) or the low-level Somali CEF (in the other three models). Either of these effects increases the rainfall over the Arabian Sea, favoring an advance in monsoon onset over the Arabian Sea under the RCP8.5 scenario.

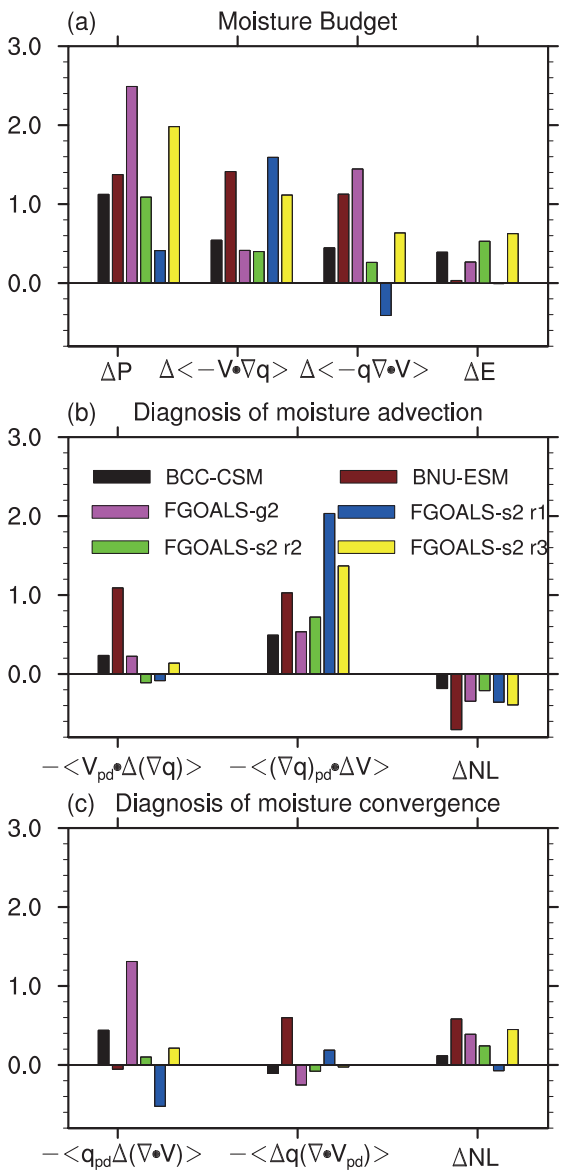

Fig. 7. (a) Moisture processes responsible for the rainfall increase (June for BNU-ESM, May for the other models) over the Arabian Sea (5°–15°N, 65°–75°E) from the relative contributions of moisture advection, moisture convergence and surface evaporation. (b) Contribution to the moisture advection by the moisture change, circulation change, and nonlinear product of the two changes. (c) Contribution to the moisture convergence by the circulation change, moisture change, and the nonlinear product of the two changes. Units: mm d^{-1}.

3.4. *Possible causes of the circulation changes*

The change in 200-hPa velocity potential matches with the change in convection over the equatorial region. Figure 8 shows the projected changes in 200-hPa velocity potential and the corresponding divergent wind field for May (June) in the results of BCC-CSM, FGOALS-g2, FGOALS-s2 (BNU-ESM) at the end of 21st century. The positive anomalies (upper-level anomalous convergences) over the eastern Indian Ocean and Maritime Continent are evident in all models with different strengths apart from in FGOALS-g2. In FGOALS-g2, the positive anomalies are found over the central and eastern equatorial Pacific.

The upper-level anomalous convergences are the indicators of the reduced convection. This is also supported by the rainfall change. In all the models except FGOALS-g2, the reduced rainfall is mainly found over the tropics between 100°E and 140°E (Fig. 6). However, in FGOALS-g2, a reduction in rainfall is evident over the central equatorial Pacific near the date line (Fig. 6c). The reduced convection in the equatorial region tends to induce anomalous local descending motion and low-level easterly flow to the west of the region, along with off-equatorial anticyclonic low-level flow farther west through the Matsuno–Gill effect (Matsuno, 1966; Gill, 1980). So, in all the models except FGOALS-g2, it is likely that the reduction in convection over the eastern Indian Ocean and Maritime Continent region drives the anomalous anticyclonic circulations over the western Indian Ocean. The much stronger low-level anomalous anticyclone over the northern Indian Ocean is ascribed to the strong easterly shear to the north of the equator (Wang and Xie, 1996; Xiang and Wang, 2013). The low-level anomalous anticyclonic circulation provides the increase in moisture advection into the Arabian Sea region. By contrast, in FGOALS-g2 the suppressed convection is farther east, such that the anomalous anticyclonic circulation is not as well defined (evidenced by the weak circulation changes over the Indian Ocean), so the increased rainfall comes more from increased moisture convergence. The low-level wind anomalous convergence over the Arabian Sea in FGOALS-g2 may be in part contributed to by the strong enhanced rainfall over the western North Indian Ocean (Fig. 6c).

The SST warming pattern is the main cause of the change in zonal atmospheric overturning circulation over the tropical Pacific Ocean (Tokinaga et al., 2012), and the precipitation changes over the tropical Pacific through the "warmer-get-wetter" mechanism (Xie et al., 2010). Figure 9 shows the future changes in SST projected by the four models, including the three realizations of FGOALS-s2 (June for BNU-ESM, but May for the other three models). The weakest warming of projected SST is found over the central equatorial Pacific in FGOALS-g2, while the strongest warming is found over the eastern equatorial Pacific in the other three models. In all the models except FGOALS-g2, the strongest warming over the eastern equatorial Pacific features a reduced zonal gradient of SST, which favors the eastward shift of atmospheric convection, with reduced convection found over the eastern Indian Ocean and Maritime Continent region, as seen in Figs. 6 and 8. In FGOALS-g2, the weakest warming over the central Pacific favors the reduction of local convection, as evidenced by reduced rainfall and upper-level anomalous convergence (Figs. 6 and 8).

Although the models (except FGOALS-g2) behave similarly in the Maritime Continent and western Indian Ocean region, they are quite different across the rest of the Pacific, even among the different members of FGOALS-s2. In

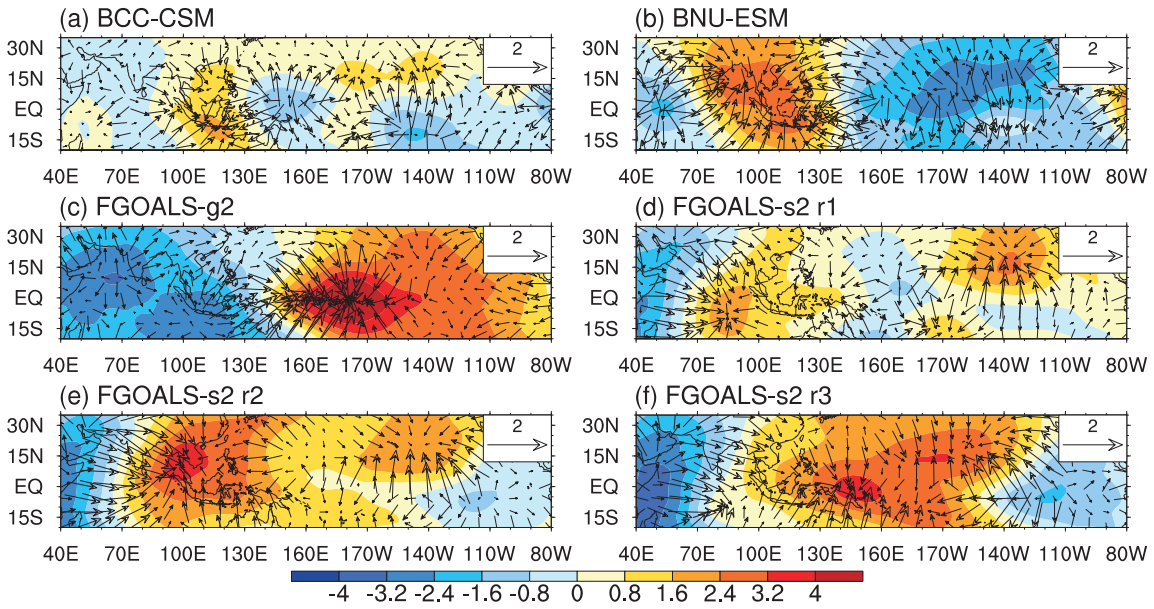

Fig. 8. As in Fig. 6 except for the 200-hPa velocity potential change (10^7 m^2 s^{-1}, shading) and corresponding divergent wind change (m s^{-1}).

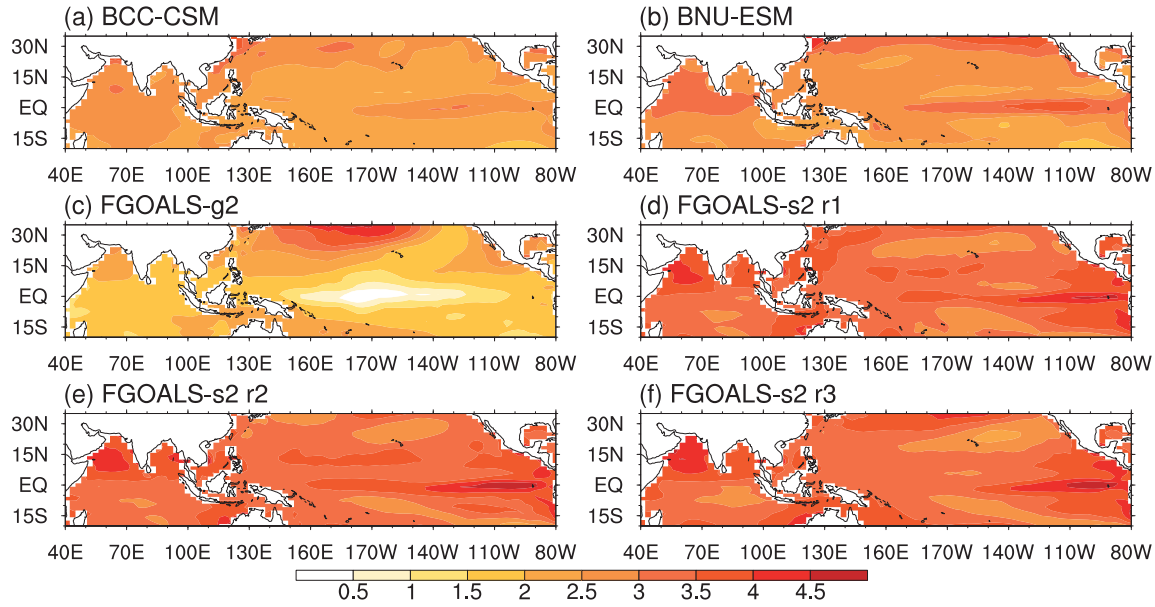

Fig. 9. As in Fig. 6 except for the SST change.

BCC-CSM and FGOALS-s2 r1, the weak upper-level anomalous divergences (negative anomalies) are found over the central equatorial Pacific and southeastern Pacific. In BNU-ESM, the whole eastern Pacific is occupied by the upper-level anomalous divergences, with the center being north of the equator at 150°W. However, in FGOALS-s2 r2 and r3 the upper-level anomalous divergences are only evident over the far eastern Pacific.

The broader-scale differences (shown in Fig. 8) may be related to the differences in the projected SST pattern and in the present-day simulations. Figure 10 shows the spatial distributions of the 200-hPa velocity potential and corresponding divergent wind for May (June) from ERA-interim, BCC-CSM, FGOALS-g2, FGOALS-s2 (BNU-ESM) in present-day climate. The observation is characterized by a deep convection around the Maritime Continent region. There are two kinds of models in terms of the location of the deep convection. In BCC-CSM and BNU-ESM the deep convections are located around the Maritime Continent region, with greater strength in BNU-ESM; whereas in FGOALS-g2 and FGOALS-s2 the deep convections are centered over the central Pacific. Consequently, compared with BNU-ESM, the eastward displacement of the projected upper-level anomalous divergences over the Pacific in FGOALS-s2 (in partic-

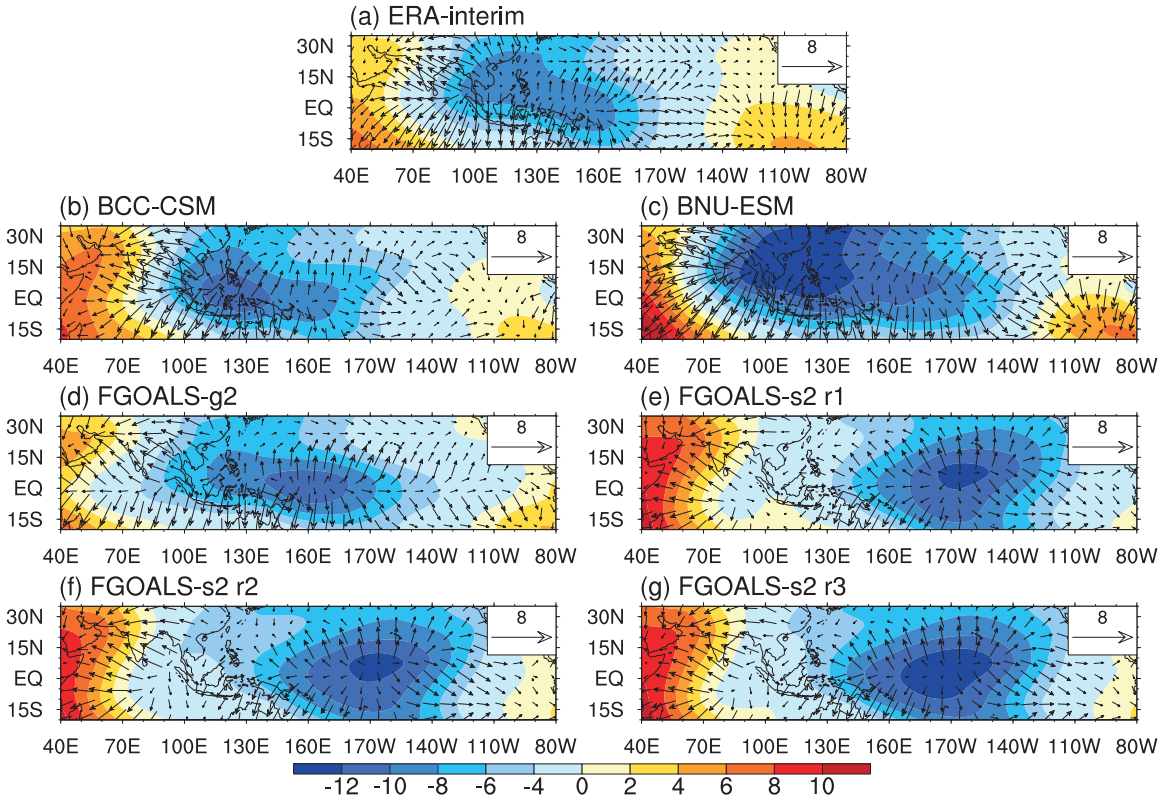

Fig. 10. Spatial distributions of the 200-hPa velocity potential (10^7 m^2 s^{-1}, shading) and corresponding divergent wind (m s^{-1}) in May (June for BNU-ESM) averaged from 1981–2005 derived from (a) ERA-interim, (b) BCC-CSM, (c) BNU-ESM, (d) FGOALS-g2, (e) FGOALS-s1 r1, (f) FGOALS-s2 r2, and (g) FGOALS-s2 r3.

ular the r2 and r3 realizations) are mainly due to the corresponding eastward shift of the deep convection under present-day conditions, given the rather similar projected SST warming pattern. The weaker projected responses in BCC-CSM are caused by both the weaker projected SST warming and the weaker deep convection around the Maritime Continent in the present-day simulation. Compared with FGOALS-s2 r1 and r2, the larger amplitude in projected changes in r3 is related to the stronger deep convection in the present-day simulation.

4. Summary and discussion

4.1. *Summary*

In this study, the reproducibility of the onset of the Asian summer monsoon by four Chinese models that participated in CMIP5 was evaluated. Three available realizations of FGOALS-s2 were also employed. The future projections under the RCP8.5 scenario derived from these four models were then analyzed. The major conclusions can be summarized as follows:

(1) The general characteristics of the onset of the Asian summer monsoon for present-day climate were reasonably captured in the four models, albeit with several differences also evident. Although FGOALS-g2 showed better skill in terms of the spatial pattern correlation coefficient, it lacked any onset over much of India, Southeast Asia and the South China Sea. All the models failed to reproduce the monsoon region over East China, Korea and Japan, and tended to simulate a delayed onset of monsoon over the Arabian Sea. The simulated much weaker low-level Somali CEFs in May weakened the moisture fluxes, resulting in dry biases over the Arabian Sea, which led to a delayed onset of the monsoon there. The biases of simulated Somali CEFs were associated with the cold biases of SST in boreal spring.

(2) The four models including the three realizations of FGOALS-s2 all projected an advanced onset of monsoon over the Arabian Sea at the end of 21st century under the RCP8.5 scenario. An increase of rainfall over the Arabian Sea, prior to the present-day onset date, favored the advanced monsoon onset in all models. The increased rainfall was accompanied by intensified local low-level westerly anomalies. The moisture budget analyses demonstrated that the increase of moisture convergence due to the increase of wind convergence played an important role in enhancing the rainfall over the Arabian Sea in FGOALS-g2, while the increase of moisture advection due to the anomalous circulation was crucial in the other three models.

(3) In all the models except FGOALS-g2, the intensified low-level westerly anomalies over the Arabian Sea were associated with the low-level anomalous anticyclone over north-

ern Indian Ocean, which was driven by the reduction in convection over the eastern Indian Ocean and Maritime continent region. By contrast, in FGOALS-g2 the anomalous anticyclonic circulation was not as well defined since the suppressed convection was farther east over the central equatorial Pacific. The low-level wind convergence anomaly over the Arabian Sea in FGOALS-g2 may have been in part contributed to by the strong enhanced rainfall over the western North Indian Ocean.

(4) In all the models except FGOALS-g2, the equatorial maximum in projected SST warming over the Pacific favored the eastward shift of atmospheric convection and then led to the reduction in convection over the eastern Indian Ocean and Maritime Continent region. However, in FGOALS-g2 the weakest warming of projected SST over the central equatorial Pacific reduced the local convection. The broader-scale differences in the projected changes by the models may have been related to the differences in the projected SST pattern and in the present-day simulations.

4.2. *Discussion*

Our suggested mechanism for the models (except FGOALS-g2) in this study is to some extent similar to the mechanisms proposed for the observed advance of the Asian summer monsoon onset since the mid-to-late 1990s. The observed onset advance occurs over a large region, extending from the Bay of Bengal to the South China Sea. Westerly wind anomalies are found from the Arabian Sea to the equatorial western North Pacific (Xiang and Wang, 2013). Modeled projected westerly anomalies also favor an advanced onset of monsoon over the Arabian Sea. The observed westerly trend is the Rossby wave response to the intensified convection to the east of the Philippines due to both the SST warming over the western Pacific and the SST cooling over the central eastern Pacific (Xiang and Wang, 2013). Modeled projected westerly anomalies are also the Rossby wave response, but to the suppressed convection over the eastern Indian Ocean and Maritime Continent region.

In addition, Wang et al. (2012) speculate that the observed early onset of monsoon over the Arabian Sea since 1997 may be caused by enhanced land–ocean thermal contrast between the Asian landmass and the equatorial Indian Ocean. Consistent increased land–ocean thermal contrast under the RCP8.5 scenario is evident in the four models examined in the present study (figure not shown) due to the large heat capacity of the oceans, but the signal with such a large scale may not be a key factor for the advanced monsoon onset over a limited region.

Finally, we only employed the model results derived from four Chinese models in this study, and gave an example of moisture budget analysis on the onset changes over the Arabian Sea. In future work we intend to use model results from more CMIP5 models to test the robustness of our findings and the suggested mechanism.

Acknowledgements. We thank the two anonymous reviewers and the editor Mike DAVEY for constructive comments that helped greatly to improve the original manuscript. This work was jointly supported by the National Natural Science Foundation of China (Grant Nos. 41330423, 41205080, and 41023002), the Carbon Budget and Related Issues project of the Chinese Academy of Sciences (Grant No. XDA05110301), and the Joint Center for Global Change Studies (Project No. 105019), Beijing, China.

REFERENCES

Adler, R. F., and Coauthors, 2003: The version-2 Global Precipitation Climatology Project (GPCP) monthly precipitation analysis (1970–present). *J. Hydrometeor.*, **4**, 1147–1167.

Bao, Q., and Coauthors, 2013: The Flexible Global Ocean-Atmosphere-Land System Model, Spectral Version 2: FGOALS-s2. *Adv. Atmos. Sci.*, **30**, 561–576, doi: 10.1007/s00376-012-2113-9.

Dee, D. P., and Coauthors, 2011: The ERA-Interim reanalysis: Configuration and performance of the data assimilation system. *Quart. J. Roy. Meteor. Soc.*, **137**, 553–597.

Ding, Q., and B. Wang, 2005: Circumglobal teleconnection in the Northern Hemisphere summer. *J. Climate*, **18**, 3483–3505.

Gill, A. E., 1980: Some simple solutions for heat-induced tropical circulation. *Quart. J. Roy. Meteor. Soc.*, **106**, 447–462.

Inoue, T., and H. Ueda, 2011: Delay of the first transition of Asian summer monsoon under global warming condition. *SOLA*, **7**, 81–84.

Kajikawa, Y., and B. Wang, 2012: Interdecadal change of the South China Sea summer monsoon onset. *J. Climate*, **25**, 3207–3218.

Kajikawa, Y., T. Yasunari, S. Yoshida, and H. Fujinami, 2012: Advanced Asian summer monsoon onset in recent decades. *Geophys. Res. Lett.*, **39**, L03803, doi: 10.1029/2011GL050540.

Kang, I. S., and Coauthors, 2002: Intercomparison of the climatological variations of Asian summer monsoon precipitation simulated by 10 GCMs. *Climate Dyn.*, **19**, 383–395.

Kitoh, A., H. Endo, K. K. Kumar, I. F. A. Cavalcanti, P. Goswami, and T. J. Zhou, 2013: Monsoons in a changing world: A regional perspective in a global context. *J. Geophys. Res. Atmos.*, **118**, 3053–3065, doi: 10.1002/jgrd.50258.

Levine, R. C., A. G. Turner, D. Marathayil, and G. M. Martin, 2013: The role of northern Arabian Sea surface temperature biases in CMIP5 model simulations and future projections of Indian summer monsoon rainfall. *Climate Dyn.*, **41**, 155–172.

Li, L. J., and Coauthors, 2013: The Flexible Global Ocean-Atmosphere-Land System Model: Grid-point Version 2: FGOALS-g2. *Adv. Atmos. Sci.*, **30**, 543–560, doi: 10.1007/s00376-012-2140-6.

Matsumoto, J., 1997: Seasonal transition of summer rainy season over Indochina and adjacent monsoon regions. *Adv. Atmos. Sci.*, **14**, 231—245, doi: 10.1007/1007/s00376-997-0022-0.

Matsuno, T., 1966: Quasi-geostrophic motions in the equatorial area. *J. Meteor. Soc. Japan*, **44**, 25–42.

Rayner, N. A., D. E. Parker, E. B. Horton, C. K. Folland, L. V. Alexander, D. P. Rowell, E. C. Kent, and A. Kaplan, 2003: Global analyses of sea surface temperature, sea ice, and night marine air temperature since the late nineteenth century. *J. Geophys. Res.*, **108**, 4407–4435, doi: 10.1029/2002JD002670.

Sperber, K. R., H. Annamalai, I. S. Kang, A. Kioth, A. Moise, A. Turner, B. Wang, and T. Zhou, 2013: The Asian summer monsoon: An intercomparison of CMIP5 vs. CMIP3 simulations of the late 20th century. *Climate Dyn.*, **41**, 2711–2744.

Tokinaga, H., S.-P. Xie, C. Deser, Y. Kosaka and Y. M. Okumura, 2012: Slowdown of the Walker circulation driven by tropical Indo-Pacific warming. *Nature*, **491**, 439–443, doi: 10.1038/nature11576.

Wang, B., and X. Xie, 1996: Low-frequency equatorial waves in vertically sheared zonal flow. Part I: Stable waves. *J. Atmos. Sci.*, **53**, 449–467.

Wang, B., and H. Lin, 2002: Rainy season of the Asian-Pacific summer monsoon. *J. Climate*, **15**, 386–398.

Wang, B., S. B. Xu, and L. G. Wu, 2012: Intensified Arabian Sea tropical storms. *Nature*, **489**, E1–E2, doi: 10.1038/nature11470.

Webster, P. J., V. O. Magana, T. N. Palmer, J. Shukla, R. A. Tomas, M. Yanai, and T. Yasunari, 1998: Monsoons: Processes, predictability, and the prospects for prediction. *J. Geophys. Res.*, **103**, 14451–14510.

Wu, T. W., and Coauthors, 2010: The Beijing climate center for atmospheric general circulation model (BCC-AGCM2.0.1): Description and its performance for the present-day climate. *Climate Dyn.*, **34**, 123–147.

Wu, T., and Coauthors, 2014: An overview of progress in climate system model development at the Beijing Climate Center applications for climate change studies. *Acta Meteorologica Sinica*, **28**, 34–56.

Wu, Q. Z., J. M. Feng, W. J. Dong, L. N. Wang, D. Y. Ji, and H. Q. B. Cheng, 2013: Introduction of the CMIP5 experiments carried out by BNU-ESM. *Advances in Climate Change Research*, **9**(4), 291–294, doi: 10.3969/j.issn.1673-1719.2013.04.008. (in Chinese)

Xiang, B. Q., and B. Wang, 2013: Mechanisms for the advanced Asian summer monsoon onset since the mid-to-late 1990s. *J. Climate*, **26**, 1993–2009.

Xie, P., and P. A. Arkin, 1997: Global precipitation: A 17-year monthly analysis based on gauge observation, satellite estimate, and numerical model outputs. *Bull. Amer. Meteor. Soc.*, **78**, 2539–2558.

Xie, S. P., C. Deser, G. A. Vecchi, J. Ma, H. Teng, and A. T. Wittenberg, 2010: Global warming pattern formation: Sea surface temperature and rainfall. *J. Climate*, **23**, 966–986.

Yu, W. D., K. P. Li, J. W. Shi, L. Liu, H. W. Wang, and Y. L. Liu, 2012: The onset of the monsoon over the Bay of Bengal: The year-to-year variations. *Atmos. Oceanic Sci. Lett.*, **5**, 342–347.

Zhang, H. Q., P. Liang, A. Moise, and L. Hanson, 2012: Diagnosing potential changes in Asian summer monsoon onset and duration in IPCC AR4 model simulations using moisture and wind indices. *Climate Dyn.*, **39**, 2465–2486.

Zhou, T. J., L. W. Zou, B. Wu, C. X. Jin, F. F. Song, X. L. Chen, and L. X. Zhang, 2014a: Development of Earth/Climate system models in China: A review from the coupled model intercomparison project perspective. *J. Meteor. Res.*, **28**(5), 762–779.

Zhou, T., and Coauthors, 2014b: Chinese contribution to CMIP5: An overview of five Chinese models' performances. *J. Meteor. Res.*, **28**(4), 481–509.